[Frontiers in Bioscience 13, 6957-6965, May 1, 2008]

Structure and stability of amyloid fibrils formed from synthetic beta-peptides

Giovanni Bellesia[1], Joan-Emma Shea[1,2]

[1]*Department of Chemistry and Biochemistry, University of California Santa Barbara, Santa Barbara, California 93106-9510, USA,* [2]*Department of Physics, University of California Santa Barbara, Santa Barbara, California 93106-9510, USA*

TABLE OF CONTENTS

1. ABSTRACT

Synthetic peptides capable of self-assembling into amyloid-like fibrillar structures are emerging as novel building blocks for biomaterials. They also serve as simple model systems to study the aggregation process involved in amyloid diseases. In this paper, we probe the structure and stability of fibrillar assemblies formed by two designed peptides P_{11}-I (CH_3-CO-$Q_2RQ_5EQ_2$-NH_2) and P_{11}-II (CH_3-CO-$Q_2RFQWQFEQ_2$-NH_2). Our results suggest that the two peptides assemble by fundamentally different mechanisms to structures of different morphologies. Coulombic interactions between charged residues Arginine and Glutamate drive the self-assembly process for peptide P_{11}-I while the hydrophobic effect appears to be the main driving force in the self-assembly of peptide P_{11}-II.

2. INTRODUCTION

The pathological aggregation of peptides and proteins into nanometer long fibrillar structures highly enriched in β-sheet content has been linked with a number of diseases, including Alzheimer's, Parkinson's and Type II diabetes (1, 2). In recent years, this inherent ability of peptides to self-assemble into large, ordered species has been exploited for the design of novel biomaterials. In particular, 4 to 30 amino acids long synthetic peptides known as "β-peptides" because of their intrinsic propensity for adopting a β-strand structure, have been shown to form assemblies strongly resembling those found in disease-related aggregation. These assemblies include β-sheet supramolecular tapes (a single β-sheet), ribbons (two tapes), fibrils (two or more ribbons) and fibers (several

fibrils). Nematic hydrogels resulting from the entanglement of these fibrillar aggregates show considerable potential for biomedical applications such as scaffolding for tissue engineering and repair, and 3D culture matrix for cell proliferation and differentiation (3, 4, 5).

Two particularly interesting model systems to probe β-peptide assembly are the eleven residue-long synthetic peptides P_{11}-I (CH_3-CO-$Q_2RQ_5EQ_2$-NH_2) and P_{11}-II (CH_3-CO-$Q_2RFQWQFEQ_2$-NH_2) designed by Boden and co-workers (6). Experimentally, these peptides undergo a concentration dependent association from random coils, to β-strands, to tapes, ribbons, fibrils and finally fibers (intertwined fibrils). TEM micrographs (6) show that mature fibrils in both P11-I and P11-II systems are about 80-Angstroms-wide, i.e. made up by 6 to 8 layers. In addition, the resulting aggregates are twisted, a result of the chirality of the single amino acids that is translated through the β-strands to the fibrils (7, 8, 9).

Peptide P_{11}-I is based on a short poly-glutamine stretch flanked by two oppositely charged residues (Arginine and Glutamate). P_{11}-I belongs to the family of *polar zippers* (10), a class of polypeptides that self-assemble into antiparallel β-sheets, β-barrels and slab-like β-crystallite assemblies (10, 11, 12, 13). Experiments on poly-glutamine sequences indicate that the side chain-side chain hydrogen bonding between Glutamine residues and Coulombic forces between oppositely charged residues (*polar zipper*) are capable of driving the aggregation process and the formation of amyloid fibrils (10, 14). As a result, ribbons and fibrils formed by stacking of P_{11}-I antiparallel β-tapes are stabilized by a network of hydrogen bonds formed between Glutamine side chain amides as well as by Coulombic interactions between Arginine and Glutamate residues.

Peptide P_{11}-II's primary sequence was designed from P_{11}-I by substituting Glutamine residues in positions 4, 6 and 8 with Phenylalanine, Tryptophan and Phenylalanine residues respectively. Although experiments on P_{11}-I show that aromatic residues are not strictly required for aggregation to occur, their presence has been shown in other systems to enhance aggregation propensity via hydrophobic and π−π interactions between aromatic residues (15). The amphiphilic nature of the P_{11}-II peptide leads to the assembly of antiparallel tapes with one hydrophobic face (QFWFQ) and to the formation of ribbons at a concentration of 0.1 mM, an order of magnitude lower than for P_{11}-I.

The experiments performed on these model systems have shed significant new light on the properties of self-assembling β-peptides. However, the low resolution of the experimental techniques used prohibits a definite structural characterization of the aggregates at an atomic level. A recent statistical mechanical model for self-assembly (6), applied to these peptides, suggested that hydrophobic forces represent the main driving factor for aggregation and that charged residues are always exposed to solvent in double tape (ribbon) structures. Short simulations (100 ps to 4 ns) were performed to test this idea, but the approximations used (very short timescales, implicit solvent, use of primitive treatment of electrostatic interactions) render these studies only partially conclusive (16, 17).

In this paper we analyze the structure and the stability of a number of ribbons and double ribbons (the smallest fibrils) formed by the peptides P_{11}-I and P_{11}-II using extensive molecular dynamics simulations with a fully atomistic description of the peptide in explicit solvent. We aim at characterizing the structural features and relative stability of ribbons and double ribbons with different interfaces. A second goal is to understand the role of side chain - side chain and hydrogen bonding, hydrophobic and Coulombic interactions in the self-assembly process.

Our findings suggest that the two peptides P_{11}-I and P_{11}-II self-assemble following different mechanisms to fibrils of different morphologies. In agreement with the predictions of the theoretical model presented in Ref. 6, we find that the hydrophobic effect appears to be the main driving force in the self-assembly of peptide P_{11}-II, and that the charged residues R and E are exposed to the solvent in double tapes (ribbons) of P_{11}-II. However, our simulations suggest that this model is not valid for the P_{11}-I system. The Coulombic forces between the charged residues Arginine and Glutamate drive the self-assembly process for peptide P_{11}-I and the most stable fibrils have the charged residues R and E buried in the fibril interface.

3. MATERIALS AND METHODS

3.1. Generation of initial configurations

Two β-peptide sequences were studied: P_{11}-I with sequence CH_3-CO-$Q_2RQ_5EQ_2$-NH_2 and P_{11}-II with sequence CH_3-CO-$Q_2RFQWQFEQ_2$-NH_2. All initial structures were generated using the Hyperchem™ software. For both the P_{11}-I and P_{11}-II peptides, single tapes were manually generated by placing 20 peptides into a planar, antiparallel β-sheet arrangement. Flat ribbons and double ribbons with different interfaces were then obtained by assembling 2 and 4 planar tapes, respectively. All ribbons and double ribbons were assembled with antiparallel relative position of the neighboring layers. A total of eight systems were considered, as listed in Table 1. The indices 1 and 2 correspond to systems related to peptides P_{11}-I and P_{11}-II, respectively. "R" denotes a ribbon and "D" a double ribbon. System R1 is an antiparallel ribbon with interface between layers composed by Glutamine residues. System R2 is an antiparallel ribbon with interface composed by Glutamine, Phenylalanine and Tryptophan residues. In both ribbons R1 and R2 the charged residues Arginine and Glutamate are exposed to the solvent. Double ribbon systems D1 and D2 are generated from direct assembly of two R1 and R2 ribbons, respectively. Systems R1, R2, D1 and D2 were predicted by the statistical mechanics model of reference 6 and the stability of these systems were examined in short (100 ps and 4 ns) MD simulations (16, 17), which made use of several approximations (implicit solvent and poor treatment of electrostatics).

Table 1. Systems considered in MD simulations

System	Peptide (sequence)	# Layers	Interface between layers
R1	$Q_2RQ_5EQ_2$	2	Q_5
R1R	$Q_2RQ_5EQ_2$	2	QRQ_2EQ
D1	$Q_2RQ_5EQ_2$	4	Q_5 : QRQ_2EQ : Q_5
D1D	$Q_2RQ_5EQ_2$	4	QRQ_2EQ : Q_5 : QRQ_2EQ
R2	$Q_2RFQWQFEQ_2$	2	QFWFQ
R2R	$Q_2RFQWQFEQ_2$	2	QRQ_2EQ
D2	$Q_2RFQWQFEQ_2$	4	QFWFQ : QRQ_2EQ : QFWFQ
D2D	$Q_2RFQWQFEQ_2$	4	QRQ_2EQ : QFWFQ : QRQ_2EQ

R denotes ribbons (double tapes) and D double ribbons. Numbers 1 and 2 refer to systems composed by peptides P_{11}-I and P_{11}-II respectively. Systems R1, R2, D1 and D2 have *standard* structure and R1R, R2R, D1D and D2D have *reversed* structure. The one-letter code for the amino acids is used throughout the table.

In addition to revisiting the stability and structural features of the R1, R2, D1 and D2 ribbons and double ribbons using extended simulations, we also consider four different arrangements in which the interface between the tapes is reversed: R1R, R2R, D1D and D2D (see Table 1 and Figure 1, which gives a pictorial representation of the interface in the different ribbon systems). Arginine, Glutamate and Glutamine residues compose the interface for both the reversed structures R1R and R2R. Double ribbon systems D1D and D2D are generated from direct assembly of two R1R and R2R ribbons, respectively.

3.2. Molecular dynamics simulations

Molecular dynamics (MD) simulations were carried out using the NAMD software (18, 19) with the CHARMM22 force field and the TIP3P water model (20). Following energy minimization for 10000 steps in vacuum, each system was solvated in a water box, with dimensions such as to maintain a minimum water layer of 7.5 Angstroms around the peptide-based structures. All the *solvated* systems underwent a second local optimization followed by a short (0.1 *ns*) NPT-MD simulation to equilibrate the box dimensions and obtain the correct water density. The final geometries obtained from the NPT-MD simulations were used as initial configurations for a final set of NVT-MD simulations.

All MD simulations were carried out under periodic boundary conditions using a time step of 2 fs. The bonds between hydrogens and the heavier atoms were constrained to their nominal lengths during integration using the RATTLE algorithm and the temperature was maintained at 300 K by coupling the system to a heat bath via the Langevin thermostat (in the NPT-MD simulations the Nose-Hoover Langevin barostat was used to maintain the system pressure at p=1 atm). Long-range electrostatic interactions were calculated by using the Ewald summation method with the Particle Mesh (PM) algorithm. The accuracy of the PM algorithm was fixed at 10-6, the order of the interpolation functions on the grid was set to 4 (cubic) and the grid size was 1.0 Angstroms. The cut-off distance in the direct space for both the van der Waals and the electrostatic interactions was 10.0 Angstroms. The total time length for each NVT-MD simulation was 30 ns. The first 10 ns were considered as equilibration while the last 20 ns were used for the calculation of all the thermodynamic and structural observables.

3.3. Definitions of structural parameters

3.3.1. Molecular chiral parameter

Structural studies by Chothia and Salemme (7, 8) showed that single strands in a β-sheet possess a right-handed twist when viewed along the backbone direction. The twist can be measured by calculating the dihedral angle $\theta(i)$ defined by the quadruplet $C_\beta(i) - C_\alpha(i) - C_\alpha(i+2) - C_\beta(i+2)$ where i refers to the i-th residue within the single strand (21). The molecular chiral parameter Θ was calculated at each time step as the average of $\theta(i)$ over both the residue index i and the total number of peptides.

3.3.2. Supramolecular chiral parameter

In different self-assembled β-peptides systems (4), the interplay between the intrinsic chirality of the single peptides and the short-ranged cohesive interactions between neighboring strands within the aggregates (mainly hydrogen bonds and side chain side chain interactions) leads to different supramolecular geometries. These geometries range from virtually flat fibrillar aggregates, when the cohesive intermolecular interactions nearly balance the chiral *deformation* of the peptides, to *helicoids* with saddle-like curvature, cylindrical helices and tubules (4, 6, 22). A left-handed circular *helicoid* is defined as a minimal surface having a left-handed circular helix as its boundary. It is characterized by a vertical symmetry axis and a regular left-handed twist along this axis. The twist angle k is related to the boundary helix pitch p by the formula $p = (2\pi / k)$. Amyloid-like fibrils that grow as left-handed helicoidal structures are characterized by a finite pitch $p = (2\pi\ d / k)$ where d is the distance between neighboring strands (~5 Angstroms) and k is the twist angle (or pitch wave number). We calculate the supramolecular chiral parameter k, directly from MD trajectories, following the procedure presented in Ref. 17. The parameter k measures the amount of local twist in the fibrils.

4. RESULTS

Conformations generated in the last 20 ns of each simulation are used for analysis. Visual inspection of the MD trajectories shows that the β-sheet nature of the ribbon and double ribbon β-sheet conformation is maintained over the length of the simulation. Average structures for the ribbons and double ribbons were calculated using the *average linkage-clustering* algorithm (23). The average structures for systems R1, R1R, D1, D1D, R2 and D2 resemble *helicoids* (defined in Section 3.3.2) with a regular, left-handed twist while systems R2R and D2D form

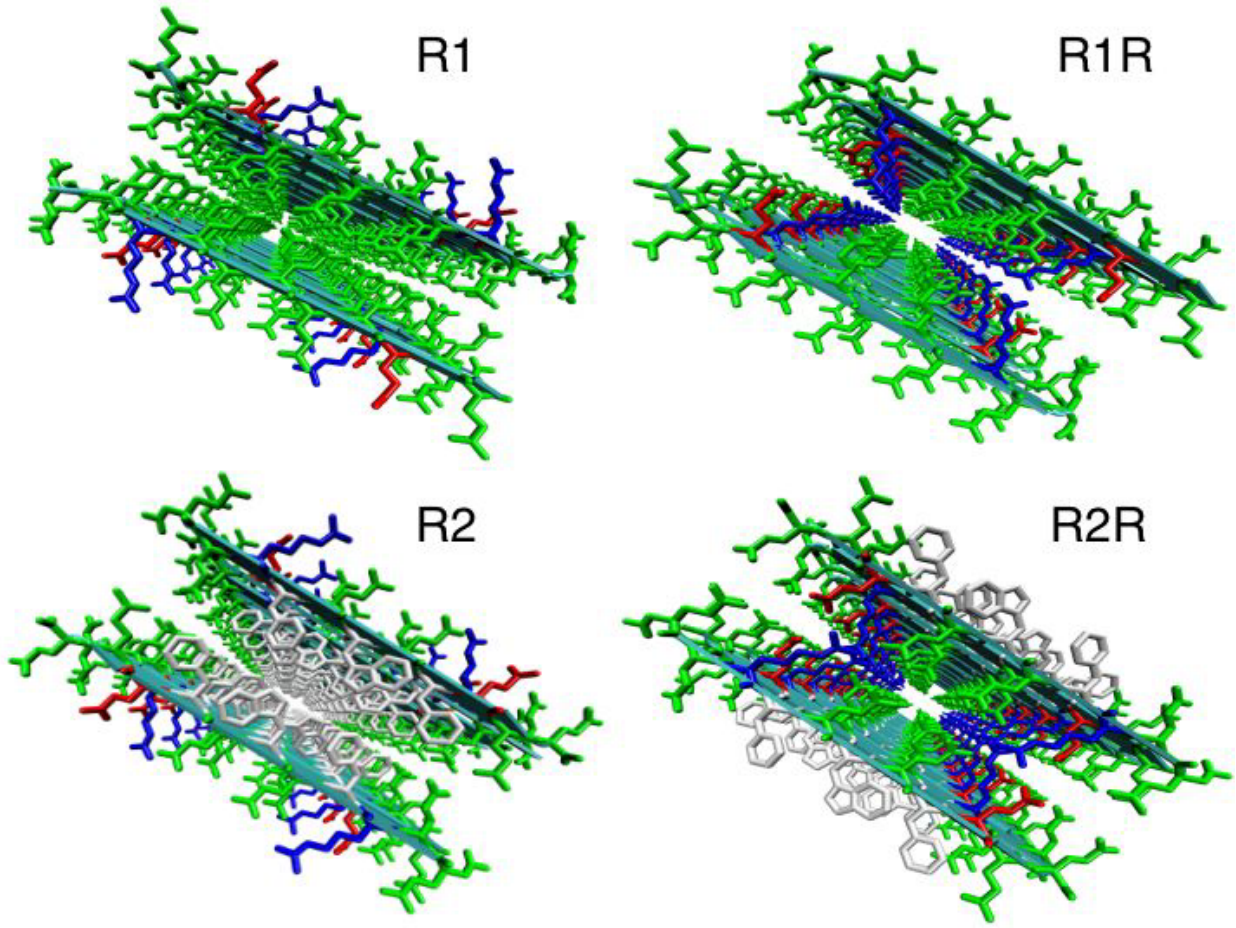

Figure 1. Schematic representation of the different interfaces for the *standard* and *reversed* ribbons. The interface for ribbon R1 (top left) is composed by Glutamine side chains (green). Tryptophan (light gray), Phenylalanine (light gray) and Glutamine side chains form the interface for ribbon R2 (bottom left). In the *reversed* ribbons R1R (top right) and R2R (bottom right) the interface is composed by Glutamine, Arginine (blue) and Glutamate (red) side chains.

straight, flat regular fibrils. The *average structures* for ribbon R2 and reversed ribbon R2R are shown in Figure 2 as a clear example of how different reciprocal arrangements of identical tapes can lead to different ribbon geometries. The R2 and R2R systems are both double antiparallel β-tapes composed by the P_{II}-II peptide, but ribbon R2 has a well-defined left-handed macroscopic twist while ribbon R2R is almost flat.

4.1. Validation of Computationally Generated Structures

A signature of amyloid fibrils is the presence of a cross-β pattern in x-ray diffraction experiments. This pattern is characterized by a meridional reflection at ~5 Angstroms, and an equatorial reflection that can range from ~7.5 to ~14 Angstroms (24, 25, 26). The meridional reflection at ~5 Angstroms corresponds to the distance between neighboring H-bonded β-strands within the same fibril layer, while the equatorial reflection corresponds to the distance between the fibril's neighboring layers. The position of this reflection depends on the size of the amino acid side chains that are packed within the layers interface.

We calculate the x-ray diffraction pattern from the average structures following the method presented in Ref. 27. Figure 3 shows the diffraction profile and a diffraction map in reciprocal space for system R1R. The corresponding plots for all other systems considered are very similar. For all the structures, both the meridional and the equatorial reflections are consistent with the cross-β structure of amyloids. Direct calculations of the interstrand and interlayer distances from the positions of the C_α atoms are also in good agreement with both the experimental and calculated x-ray diffraction results. Time average values for the interstrand distance in ribbons and double ribbons vary between 4.8 and 4.9 Angstroms while the interlayer distance varies between 9.5 and 15.2 Angstroms.

In agreement with x-ray diffraction-based studies, our coordinate-based calculations show that the interlayer distance is small (~9 to ~11 Angstroms) when Glutamine residues compose the interface between the layers, as in system R1. On the other hand, larger values for the interlayer distance are observed either when Arginine and Glutamate or when the aromatic residues are buried from

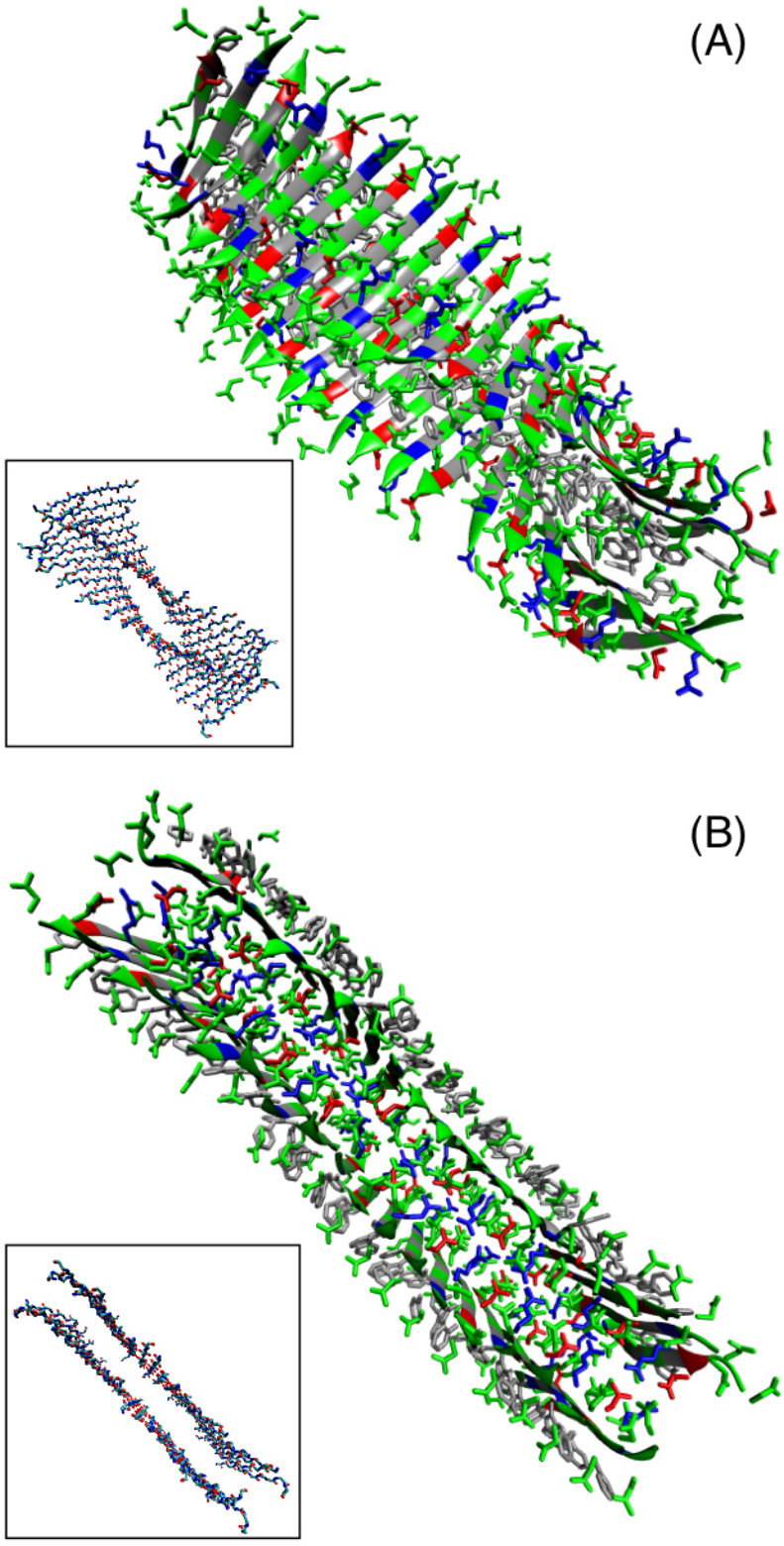

Figure 2. Different reciprocal arrangements of identical tapes composed by peptide $P_{11}II$ lead to different ribbon geometries. (A) Representative structure for system R2. The chirality of the single strands is translated to the supramolecular level of the ribbon. As a result the ribbon has a left-handed macroscopic twist. (B) Representative structure for system R2R. Strong cohesive surface-surface and surface-water interactions (originating mainly from aromatic residues) counterbalance the chiral deformation of the single strands and the ribbon appears almost flat.

.

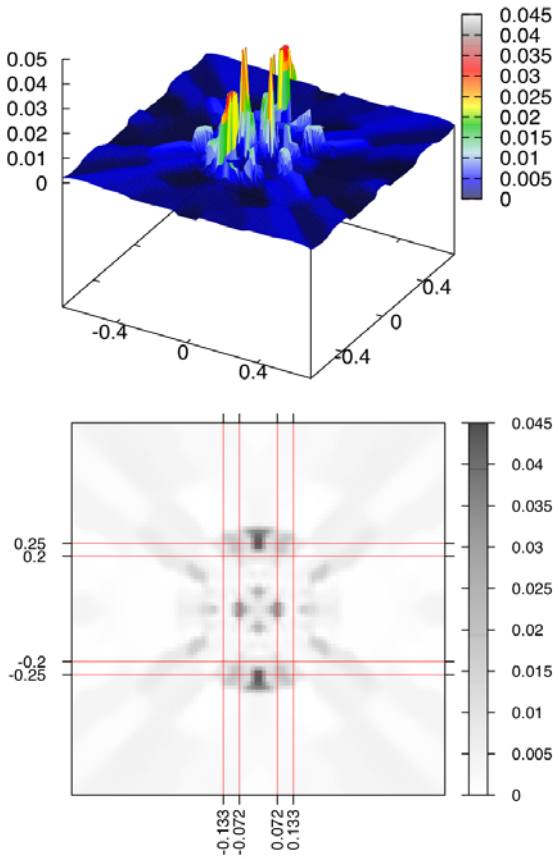

Figure 3. Example of an x-ray diffraction pattern calculated from the average structure of system R1R. Top: Profile view of the x-ray diffraction pattern. The four main peaks correspond to the equatorial and the meridional reflections. Bottom: Map view of the x-ray diffraction pattern. The horizontal and the vertical lines define the meridional and the equatorial reflection intervals compatible with the cross-β pattern. Units in the reciprocal space are Angstroms^{-1}.

the solvent and packed within the interface, as in systems R1R, R2 and R2R.

4.2. Stability

The stability of the different systems was assessed by calculating the RMSD from the average structure. Plots of the RMSD as a function of time in Figure 4 show that all the structures are stable over the simulation time and that the stability increases with the complexity of the aggregate (from ribbon to double ribbon). Interestingly, ribbons with different interfaces have almost identical RMSD (as can be seen in both the time series and the average values in Figure 4), indicating that RMSD alone cannot distinguish between *standard* (R1, R2, D1, D2) and *reversed* (R1R, R2R, D1D, D2D) structures. In order to differentiate between the two arrangements, we calculated protein-protein and protein-water non-bonded potential energy values (shown in Table 2), which indicate that *reversed* structures have slightly lower protein-protein potential energy if compared to their corresponding *standard* structures. The protein-water potential energy follows the same trend for the P_{11}-I systems. For the P_{11}-II systems, on the other hand, protein-water interactions seem to favor *standard* structures over *reversed* ones. A more detailed view of both protein-protein and protein-water non-bonded potential energy is given in Table 3 where we present the results for interface and surface potential energy in ribbons. If we consider that the entropic contribution to the free energy is the same for structures composed of the same peptide (P_{11}-I or P_{11}-II) and having the same number of layers, then we can conclude from our analysis of the potential energy contributions (Tables 2 and 3) that:

(a) For the P_{11}-I systems, the *reversed* structures R1R and D1D are more stable than the *standard* structures R1 and D1, respectively. Data in Table 3 show that the additional stability of the *reversed* structures is mainly due to strong Coulombic interactions between ARG and GLU residues at the interface level (see $< PE_{INT} >$ for systems R1 and R1R). The contribution of the charged amino acids to the stability of the ribbon interface overcomes the energetic cost originating from the burial of the same amino acids from the solvent ($< PE_{SURF\text{-}W} >$ and $< PE_{SURF\text{-}SURF} >$ for systems R1 and R1R).

(b) For the P11-II systems the standard ribbon R2 appears to be more stable than the reversed one (R2R). This is consistent with experimental results (6). Data in Table 3

Table 2. Protein internal potential energy (PE_{PP}) and protein-water potential energy (PE_{PW})

System	$< PE_{PP} >$	$< PE_{PW} >$	$< PE_{PP} > + < PE_{PW} >$
R1	-31187 (30)	-9323 (66)	-40510 (96)
R1R	-32035 (15)	-9866 (39)	-41901 (54)
D1	-64705 (34)	-18485 (31)	-83190 (65)
D1D	-65986 (27)	-18764 (28)	-84750 (55)
R2	-24848 (7)	-11337 (17)	-36185 (24)
R2R	-26060 (22)	-7996 (36)	-34056 (58)
D2	-52289 (22)	-15965 (37)	-68254 (59)
D2D	-52816 (24)	-16803 (27)	-69619 (51)

Time averages are obtained from MD simulations. Errors are in brackets; all quantities are expressed in Kcal/mol.

Table 3. Protein interface (PE_{INT}), protein surface-water (PE_{SURF-W}) and protein surface ($PE_{SURF-SURF}$) potential energies

System	$< PE_{INT} >$	$< PE_{SURF-W} >$	$< PE_{INT} > + < PE_{SURF-W} >$	$< PE_{SURF-SURF} >$
R1	-681.8 (3.2)	-4082.4 (9.0)	-4764.2 (12.2)	-12048.9 (4.1)
R1R	-1888.1 (7.0)	-3116.1 (7.8)	-5004.2 (14.8)	-9280.5 (3.2)
R2	-477.1 (1.4)	-7449.8 (11.6)	-7926.9 (13.0)	-19129.5 (6.2)
R2R	-1743.3 (7.5)	-1749.1 (5.6)	-3492.4 (13.1)	-3025.6 (2.3)

The interface and surface potential energies have been calculated considering side chain atoms only. Time averages are obtained from MD simulations. Errors are in brackets; all quantities are expressed in Kcal/mol.

show that there is a large energetic cost for packing the bulky aromatic residues within the ribbon interface (see < PEINT >, system R2). However, the largest energy cost in P11-II systems stems from the exposure of the aromatic residues to the solvent (see < PEINT >, system R2). The hydrophobic effect involving aromatic residues is strong enough to overcome the unfavorable energy of packing. It is worth noting that the standard double ribbon D2 is the only structure for which the sum of protein-protein and protein-water potential energy is less than twice that of the corresponding ribbon structure R2. This is mainly due to unfavorable protein-water potential energy (see Table 2).

4.3. Chirality

In Table 4 we present the results for the molecular chiral parameter Θ and for the pitch wave number k (positive and negative values are associated to right- and left-handedness, respectively). The calculated pitch wave number k is in good agreement with experimental data from EM micrographs and x-ray diffraction (6). A comparison of the molecular and supramolecular chiral parameters reveals a clear monotonic dependence of the macroscopic twist of the tapes (pitch wave number k) on the degree of *chiral* deformation (parameter Θ) of the single peptides; a larger *chiral* deformation of the strands leads to a larger macroscopic twist. There is also overall consistency between the sign of the parameter Θ and the sign of the pitch wave number k. In addition, the data in Table 4 show that double ribbons are less twisted when compared to their *corresponding* ribbon structures and also confirm that different mutual arrangements of identical β-tapes may result in ribbons with different macroscopic twists (see Figure 1).

5. DISCUSSION

In this paper we study the stability of several amyloid-like structures formed by two glutamine-based synthetic peptides, P_{11}-I and P_{11}-II, by means of molecular dynamics simulations. Our results suggest two different mechanisms for the self-assembly of these two peptides into fibrils of different morphologies.

Peptide P_{11}-I is a glutamine-based *polar zipper* and the main driving force in ribbon formation appears to be electrostatic in origin, involving the charged amino acids Arginine and Glutamate. Our results show that this strong Coulombic interaction together with the attractive forces between Glutamine side chains is responsible for the stabilization of the fibrils. Our simulations clearly indicate that the most stable fibrils are those in which the two charged residues are buried in the interface and not exposed to solvent (the *reversed* structures R1R and D1D). This result is in contrast to the predictions of a generic theoretical self-assembly model proposed in Ref. 6. In that model, the authors propose, based on considerations of *surface self-affinity* and *solvent affinity* of the different side groups, that the charged amino acids Arginine and Glutamate are always exposed to the solvent in ribbons formed by peptide P11-I and that glutamine side chain interactions alone stabilize the ribbon interface. It should be noted that there is no direct experimental verification of their proposed structure. Indeed, experiments performed on those peptides could not distinguish between standard and reversed arrangements of the layers constituting the fibrils. We note that it is possible that both *reversed* and *standard* fibrils are present in experiments (both constructs were stable in simulation based on RMSD from the average structure). We observed this type of coexistence of fibrils consisting of different interfaces in our recent simulations using a coarse grained peptide model (28).

Peptide P_{11}-II's sequence has been designed to increase the tendency to form ribbons through the substitution of three Glutamine residues in peptide P_{11}-I with three aromatic residues: Phenylalanine in positions 4 and 8, and Tryptophan in position 6. Experiments on peptide P_{11}-II confirm that the presence of the aromatic residues enhances ribbon formation (6). Our results indicate that ribbons based on peptide P_{11}-II are mainly stabilized by *hydrophobic* interactions. Indeed, we observe a high, unfavorable surface energy contribution when aromatic residues are exposed to the solvent.

Table 4. Time average of the intramolecular helicity parameter Θ and of the twist angle *k* obtained from MD simulations

System	< Θ >	< *k* >
R2	13.3 (0.1)	-7.5 (0.1)
R1	11.3 (0.1)	-5.0 (0.1)
R1R	10.8 (0.1)	-4.1 (0.1)
D1	9.9 (0.1)	-3.8 (0.1)
D1D	5.9 (0.1)	-2.5 (0.1)
D2	4.7 (0.1)	-2.3 (0.1)
R2R	3.8 (0.1)	-1.3 (0.1)
D2D	1.5 (0.1)	-0.6 (0.1)

Data are ordered to show the monotonic correspondence between Θ and *k*. A larger *chiral* deformation of the strands (Θ) corresponds to a larger twist magnitude. Positive and negative values are associated to right- and left-handedness, respectively. Errors are in brackets; all quantities are expressed in degrees.

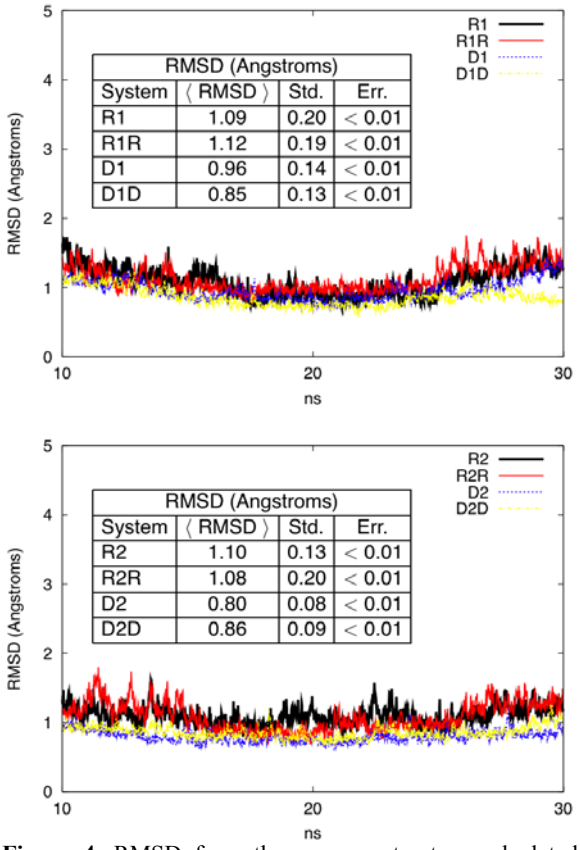

Figure 4. RMSD from the average structure calculated over the last 20 *ns*. Top: systems R1, R1R, D1, D1D. Bottom: R2, R2R, D2, D2D. Both the time series and the time average of the RMSD show that there is a small increase in the stability from ribbons to double ribbons. RMSD calculations do not distinguish between *standard* and *reversed* structures.

Our simulations show that different reciprocal arrangements of identical tapes lead to supramolecular structures with different geometries. A similar observation has been made in the case of the Alzheimer Amyloid-beta $A\beta_{16\text{-}22}$ peptide (22, 27). While the equilibrated structures generated in our simulations differ in overall morphology, they share the following features: absence of bending of the fibrils (i.e. a vertical axis of symmetry) and a regular left-handed twist. The absence of bending is related to the fact that the systems considered in our simulations have identical outer faces. Hence, the surface forces are symmetric and there is no preferential bending toward any of the two faces of the fibril. Indeed, individual tapes of P11-I peptide seen in experiment (6) possess a helical geometry with finite twist and bend due to the different chemical nature of the two faces of the tape (QRQQEQ and QQQQQ respectively). 30 ns long MD simulations confirm that the single P11-I β-tape resembles a cylindrical helix, with bending towards the face composed by residues QRQQEQ (data not shown). The left-handed twist common to all the structures analyzed in this study is related to the chiral deformation of the single peptides caused by the intrinsic property of the main chain to twist in the right-hand direction (21). Its magnitude varies from 7.5 degrees in the highly twisted R2 ribbon to 0.6 degrees in the almost flat D2D double ribbon. There is a large variation in the twist among the different structures due to the complex interplay between the main chain *chiral forces* and side chain- side chain interactions.

6. ACKNOWLEDGMENTS

The authors would like to thank Nazario Tantalo for providing the code for the x-ray diffraction calculations. This work is supported by funds from the David and Lucile Packard Foundation and the NSF grant #MCB0642086.

7. REFERENCES

1. Louise C. Serpell, Margareth Sunde, Colin C.F. Blake: The molecular basis of amyloidoses. *CMLS* 53, 871-887 (1997)
2. David G. Lynn, Steve C. Meredith: Review: Model peptides and the physicochemical approach to β-amyloids. *J. Struct. Biol.* 130, 153-173 (2000)
3. Shuguang Zhang : Emerging biological materials through molecular self-assembly. *Biotechnol. Adv.* 20, 321-339 (2002)
4. Shuguang Zhang: Fabrication of novel biomaterials through molecular self-assembly. *Nat. Biotechnol.* 21(10), 1171-1177 (2003)
5. Karthikan Rajagopal, Joel P. Schneider: Self-assembling peptides and proteins for nanotechnological applications. *Curr. Opin. in Struct. Biol.* 14, 480-486 (2004)
6. Amalia Aggeli, Irina A. Nyrkova, Mark Bell, Richard Harding, Lisa M. Carrick, Tom C.B. McLeish, Alexander N. Semenov, Neville Boden: Hierarchical self-assembly of chiral rod-like molecules as a model for peptide β-sheet tapes, ribbons, fibrils and fibers. *Proc. Nat. Acad. Sci. U.S.A.* 98(21), 11857-11862 (2001)
7. Cyrus Chothia : Conformation of twisted β-pleated sheets in proteins. *J. Mol. Biol.* 75, 295-302 (1973)
8. D.W. Weatherford, F. Raymond Salemme: Conformation of twisted parallel β-sheets and the origin of chirality in protein structures. *Proc. Nat. Acad. Sci. U.S.A.* 76(1), 19-23 (1979)

9. Jonathan Selinger, Mark S. Spector, Joel M. Schnur: Theory of self-assembled tubules and helical ribbons. *J. Phys. Chem. B* 105(30), 7157-7169 (2001)
10. Max F. Perutz, Tony Johnson, Masashi Suzuki, John T. Finch: Glutamine repeats as polar zippers: Their possible role in inherited neurodegenerative diseases. *Proc. Nat. Acad. Sci. U.S.A.* 91, 5355-5358 (1994)
11. Max F. Perutz, John T. Finch, John Berriman & Arthur Lesk: Amyloid fibers are water-filled nanotubes. *Proc. Nat. Acad. Sci. U.S.A.* 99(8), 5591-5595 (2002)
12. Christopher A. Ross, Michelle A. Poirier, Erich E. Wanker, Mario Amzel: Polyglutamine fibrillogenesis: The pathway unfolds. *Proc. Nat. Acad. Sci. U.S.A.* 100(1), 1-3 (2003)
13. Deepak Sharma, Leonid M. Shinchuk, Hideyo Inouye, Ronald Wetzel, Daniel A. Kirschner: Polyglutamine homopolymers having 8-45 residues form slablike β-crystallite assemblies. *PROTEINS: Struct. Funct. Bioinf.* 61, 398-411 (2005)
14. Lars Tjernberg, Waltteri Hosia, Niklas Bark, Johan Thyberg, Jan Johansson: Charge attraction and β propensity are necessary for amyloid fibril formation from tetrapeptides. *J. Biol. Chem.* 277(45), 43243-43246 (2002)
15. Ehud Gazit: A possible role for pi-stacking in the self-assembly of amyloid fibrils. *FASEB J.* 16, 77-83 (2002)
16. Colin W.G. Fishwick, Andrew J. Beevers, Lisa M. Carrick, Conor D. Whitehouse, Amalia Aggeli, Neville Boden: Structures of helical β-tapes and twisted ribbons: The role of side-chain interactions on twist and bend behaviour. *Nano Lett.* 3(11), 1475-1479 (2003)
17. Giovanni Bellesia, Maxim V. Fedorov, Edward G. Timoshenko: Molecular dynamics study of structural properties of β-sheet assemblies formed by synthetic de novo oligopeptides. *Physica A* 373, 455-476 (2007)
18. Jim C. Phillips, Rosemary Braun, Wei Wang, James Gumbart, Emad Tajkhorshid, Elizabeth Villa, Christophe Chipot, Robert D. Skeel, Laxmikant Kale, Klaus Schulten: Scalable molecular dynamics with NAMD. *J. Comput. Chem.* 26, 1781-1802 (2005)
19. NAMD was developed by the Theoretical and Computational Biophysics Group in the Beckman Institute for Advanced Science and Technology at the University of Illinois at Urbana-Champaign
20. Alexander D. MacKerell, Jr., Donald Bashford, M. Bellott, Roland L. Dunbrack Jr., Jeffrey D. Evanseck, M.J. Field, Stefan Fischer, Jiali Gao, H. Guo, Sookhee Ha, Diane Joseph-McCarthy, L. Kuchnir, Krzysztof Kuczera, Frankie T.K. Lau, Carla Mattos, Stephen Michnick, T. Ngo, Dzung T. Nguyen, Blaise Prodhom, Walter E. Reiher III, Benoit Roux, M. Schlenkrich, J.C. Smith, Roland Stote, John Straub, Masakatsu Watanabe, Joanna Wiorkiewicz-Kuczera, D. Yin, Martin Karplus: All-atom empirical potential for molecular modeling and dynamics studies of proteins. *J. Phys. Chem. B* 102, 3586-3616 (1998)
21. Igor L. Shamovsky, Gregory M. Ross, Richard J. Riopelle: Theoretical studies on the origin of the β-sheet twisting. *J. Phys. Chem. B* 104, 11296-11307 (2000)
22. Kun Lu, Jaby Jacob, Pappannan Thiyagarajan, Vincent P. Conticello, David G. Lynn: Exploiting amyloid fibril lamination for nanotube self-assembly. *J. Am. Chem. Soc.* 125(21), 6391-6393 (2003)
23. Stephen C. Johnson: Hierarchical Clustering Schemes. *Psychometrika* 2, 241-254 (1967)
24. Rebecca Nelson, Michael R. Sawaya, Melinda Balbirnie, Anders O. Madsen, Christian Riekel, Robert Grothe, David Eisemberg: Structure of the cross-β spine of amyloid-like fibrils. *Nature* 435, 773-778 (2005)
25. Steve C. Meredith: Protein denaturation and aggregation. *Ann. N.Y. Acad. Sci.* 1066, 181-221 (2005)
26. Pavel Sikorski, Edward D.T. Atkins, Louise C. Serpell: Structure and texture of fibrous crystals formed by Alzheimer Aβ(11-25) peptide fragment. *Structure* 11, 915-926 (2003)
27. Ute F. Rohrig, Alessandro Laio, Nazario Tantalo, Michele Parrinello, Roberto Petronzio: Stability and structure of oligomers of the Alzheimer peptide $A\beta_{16-22}$: from the dimer to the 32-mer. *Biophys. J.* 91, 3217-3229 (2006)
28. Giovanni Bellesia, Joan-Emma Shea: Self-assembly of beta-sheet forming peptides into chiral fibrillar aggregates. *J. Chem. Phys.* 126, 245104 (2007)

Abbreviations: BSE: bovine spongiform encephalopathy, CJD: Creutzfeldt-Jakob disease, MD: molecular dynamics, PM: particle mesh, RMSD: root mean square deviation

Key Words: Peptides, Aggregation, Amyloids, Molecular Dynamics, Stability, Chirality

Send correspondence to: Joan-Emma Shea, Department of Chemistry and Biochemistry, University of California, Santa Barbara, Santa Barbara, CA 93106, Tel: 805-893-5604, Fax: 805-893-4120, E-mail: shea@chem.ucsb.edu

http://www.bioscience.org/current/vol13.htm